Sandia National Laboratories

SAND2018-10665C

Time-Dependent Density Functional Theory for High Energy Density Physics

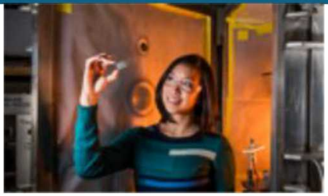

Stopping Power* in Warm Dense Targets from First Principles

*** and more**

PRESENTED BY

Attila Cangi, D. S. Jensen, S. B. Hansen, A. D. Baczewski

16th International Conference on the Physics of Non-Ideal Plasmas, Saint-Malo, France, September 28, 2018

U.S. Department of Energy NNSA

Sandia National Laboratories is a multimission laboratory managed and operated by National Technology & Engineering Solutions of Sandia, LLC, a wholly owned subsidiary of Honeywell International Inc., for the U.S. Department of Energy's National Nuclear Security Administration under contract DE-NA0003525.

Introduction

Interplay of Theory, Simulation, and Experiment in HED Physics


PRL 113, 155003 (2014) PHYSICAL REVIEW LETTERS week ending 10 OCTOBER 2014

Experimental Demonstration of Fusion-Relevant Conditions in Magnetized Liner Inertial Fusion

M. R. Gomez, S. A. Slutz, A. B. Sefkow, D. B. Sinars, K. D. Hahn, S. B. Hansen, E. C. Harding, P. F. Knapp, P. F. Schmit, C. A. Jennings, T. J. Awe, M. Geissel, D. C. Rovang, G. A. Chandler, G. W. Cooper, M. E. Cuneo, A. J. Harvey-Thompson, M. C. Herrmann, M. H. Hess, O. Johns, D. C. Lamppa, M. R. Martin, R. D. McBride, K. J. Peterson, J. L. Porter, G. K. Robertson, G. A. Rochau, C. L. Ruiz, M. E. Savage, I. C. Smith, W. A. Stygar, and R. A. Vesey

Sandia National Laboratories, P.O. Box 5800, Albuquerque, New Mexico 87185, USA

(Received 18 June 2014; published 6 October 2014)

HED experiments

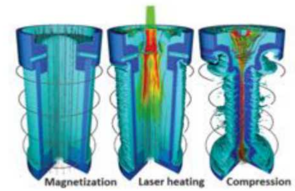

Magneto-hydrodynamics simulations support design of HED experiments.

HED experiments and diagnostics provide data to benchmark theory.

Magneto-hydrodynamics simulations

AMO/Electronic structure theory

Atom/Electronic structure theory provides data on microscopic scale (electronic transport properties) as input to magneto-hydrodynamics simulations.

Introduction

Utility of TDDFT for HED physics

Electronic Structure and Condensed Matter Theory

DFT		TDDFT			AMO Physics
Equation of state	Shock physics	Stopping Power	Conductivities	Dynamic Structure Factor	

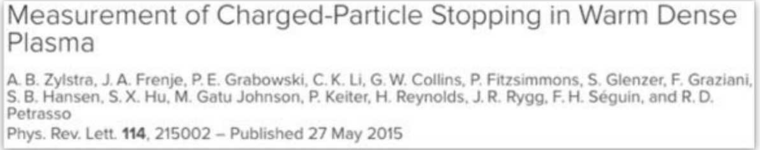

Measurement of Charged-Particle Stopping in Warm Dense Plasma

A. B. Zylstra, J. A. Frenje, P. E. Grabowski, C. K. Li, G. W. Collins, P. Fitzsimmons, S. Glenzer, F. Graziani, S. B. Hansen, S. X. Hu, M. Gatu Johnson, P. Keiter, H. Reynolds, J. R. Rygg, F. H. Séguin, and R. D. Petrasso

Phys. Rev. Lett. **114**, 215002 – Published 27 May 2015

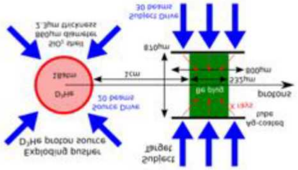

$$\frac{\partial E}{\partial x} = \frac{1}{v}\frac{\partial}{\partial t}\langle E \rangle$$

Free-Electron X-Ray Laser Measurements of Collisional-Damped Plasmons in Isochorically Heated Warm Dense Matter

P. Sperling, E. J. Gamboa, H. J. Lee, H. K. Chung, E. Galtier, Y. Omarbakiyeva, H. Reinholz, G. Röpke, U. Zastrau, J. Hastings, L. B. Fletcher, and S. H. Glenzer

Phys. Rev. Lett. **115**, 115001 – Published 9 September 2015

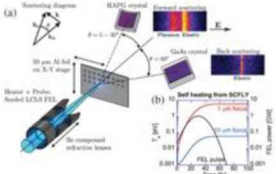

$$\sigma(\omega) = \frac{\mathbf{J}(\omega)}{\mathbf{E}(\omega)}$$

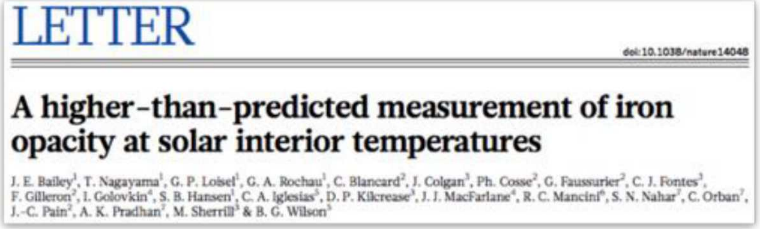

LETTER

doi:10.1038/nature14048

A higher-than-predicted measurement of iron opacity at solar interior temperatures

J. E. Bailey[1], T. Nagayama[1], G. P. Loisel[1], G. A. Rochau[1], C. Blancard[2], J. Colgan[3], Ph. Cosse[2], G. Faussurier[2], C. J. Fontes[3], F. Gilleron[2], I. Golovkin[4], S. B. Hansen[1], C. A. Iglesias[5], D. P. Kilcrease[3], J. J. MacFarlane[4], R. C. Mancini[6], S. N. Nahar[7], C. Orban[7], J.-C. Pain[2], A. K. Pradhan[7], M. Sherrill[3] & B. G. Wilson[5]

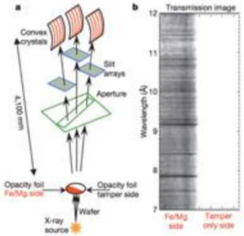

$$S(\mathbf{q},\omega) = -\frac{1}{\pi}\frac{\Im[\chi(\mathbf{q},-\mathbf{q},\omega)]}{1-e^{-\omega/k_{\mathrm{B}}T}}$$

Introduction

Coupled Electron-Ion Many-Body Problem

Time-dependent Schrödinger equation for the many-particle (molecular) Hamiltonian.

$$i\hbar \frac{\partial}{\partial t} \Psi(\{\mathbf{R}\}, \{\mathbf{r}\}, t) = \hat{H} \Psi(\{\mathbf{R}\}, \{\mathbf{r}\}, t)$$

$$\hat{H} = \hat{T}^n + \hat{W}^{nn} + \hat{T}^e + \hat{W}^{ee} + \hat{W}^{en} + \hat{V}^n + \hat{V}^e$$

Kinetic, interaction, and external potential terms.

$$\hat{T}^n = \sum_{\alpha}^{N^n} -\frac{\hbar^2}{2M_\alpha} \nabla_\alpha^2 \qquad \hat{T}^e = \sum_{i}^{N^e} -\frac{\hbar^2}{2m} \nabla_i^2$$

$$\hat{W}^{nn} = \frac{1}{2} \sum_{\alpha,\beta,\alpha\neq\beta}^{N^n} \frac{e^2 \, Z_\alpha \, Z_\beta}{4\pi\epsilon_0 \, |\mathbf{R}_\alpha - \mathbf{R}_\beta|} \qquad \hat{W}^{ee} = \frac{1}{2} \sum_{i,j,i\neq j}^{N^e} \frac{e^2}{4\pi\epsilon_0 \, |\mathbf{r}_i - \mathbf{r}_j|} \qquad \hat{W}^{en} = -\sum_{i}^{N^e} \sum_{\alpha}^{N^n} \frac{e^2 \, Z_\alpha}{4\pi\epsilon_0 \, |\mathbf{r}_i - \mathbf{R}_\alpha|}$$

$$\hat{V}^n = \sum_{\alpha}^{N^n} v^n(\mathbf{R}_\alpha) \qquad \hat{V}^e = \sum_{i}^{N^e} v^e(\mathbf{r}_i)$$

Introduction
Time-dependent DFT and Ehrenfest MD

We reduce the complexity to a one-body problem (somewhat at the cost of accuracy).

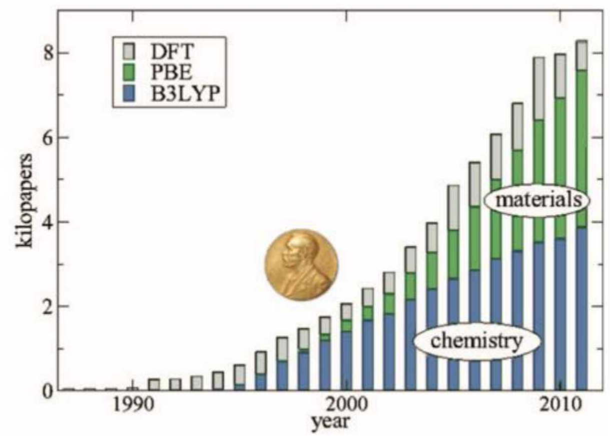

K. Burke, J. Chem. Phys. **136**, 150901 (2012).

Two coupled equations of motion

- TD Kohn-Sham equations

$$i\frac{\partial}{\partial t}\phi_i(\mathbf{r},t) = \left\{-\frac{1}{2}\nabla^2 + v_{\mathrm{S}}(\mathbf{r},t)\right\}\phi_i(\mathbf{r},t)$$

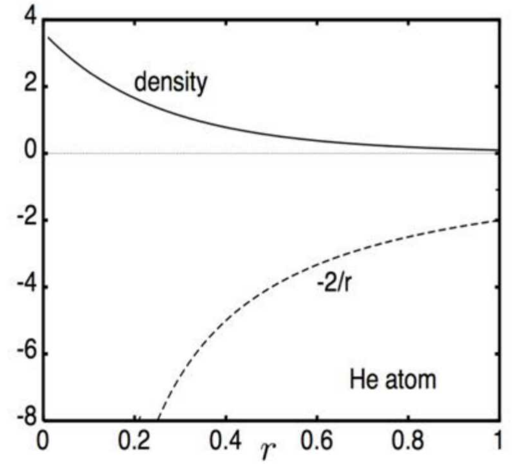

- Ehrenfest MD

$$M_\alpha \frac{\partial^2 \mathbf{R}_\alpha}{\partial t^2} = -\nabla_{R_\alpha} E[R_\alpha, n(\mathbf{r},t)]$$

The ABC of DFT (dft.uci.edu/doc/g1.pdf).

Introduction

Implementation of TDDFT for HED

Sandia implementation of TDDFT-Ehrenfest MD in VASP

- Andrew D. Baczewski et al., PRL **116**, 115004 (2016)
- Plane wave basis
- Projector-augmented wave (PAW) formalism
- Crank-Nicolson time integration (unitary)
- Generalized minimal residual method

Scales well on DOE machines

- Typically 100s of cores, a few hours
- No "free" parameters
  - takes mass density
  - # of electrons
  - exchange-correlation functional

$$i\frac{\partial}{\partial t}\phi_i(\mathbf{r},t) = \left\{-\frac{1}{2}\nabla^2 + v_{\mathrm{S}}(\mathbf{r},t)\right\}\phi_i(\mathbf{r},t)$$

$$M_\alpha \frac{\partial^2 \mathbf{R}_\alpha}{\partial t^2} = -\nabla_{R_\alpha} E[R_\alpha, n(\mathbf{r},t)]$$

$$\vec{F}_\alpha = \sum_{nqq'} f_n \mathbf{C}^*_{nq'}(t)\left[\nabla_{R_\alpha}\mathbf{H}_{\mathrm{S}} - \epsilon_n \mathbf{S}\right]\mathbf{C}_{nq}(t)$$

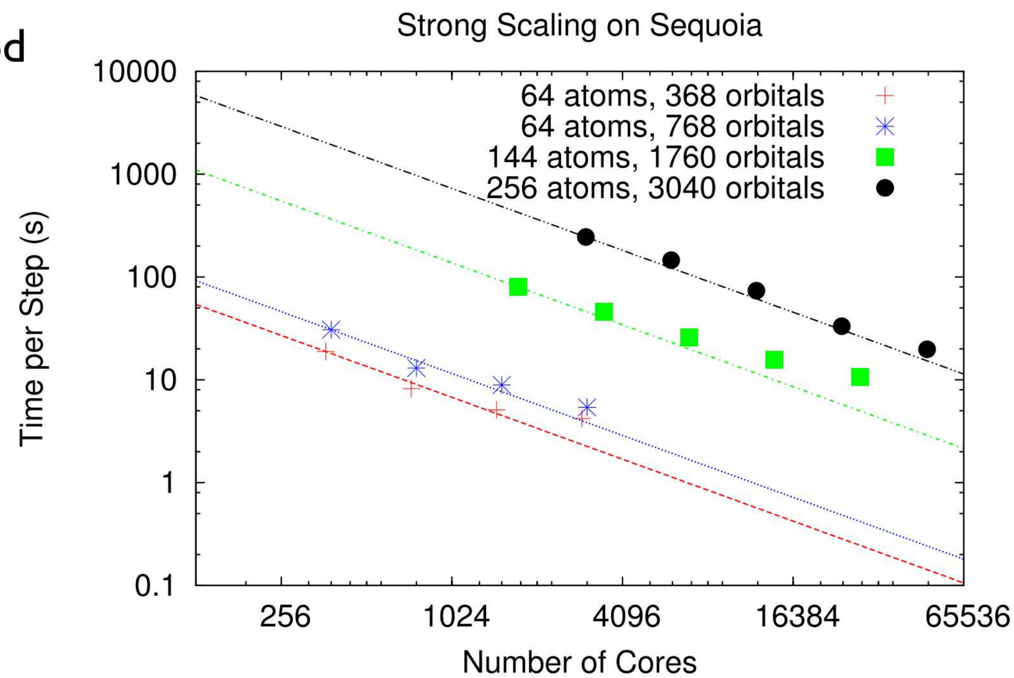

Stopping Power

Importance of Non-Adiabatic Effects

Hydrogen moving through cold, bulk aluminum in a channeling trajectory

Projectile velocity

Born-Oppenheimer MD

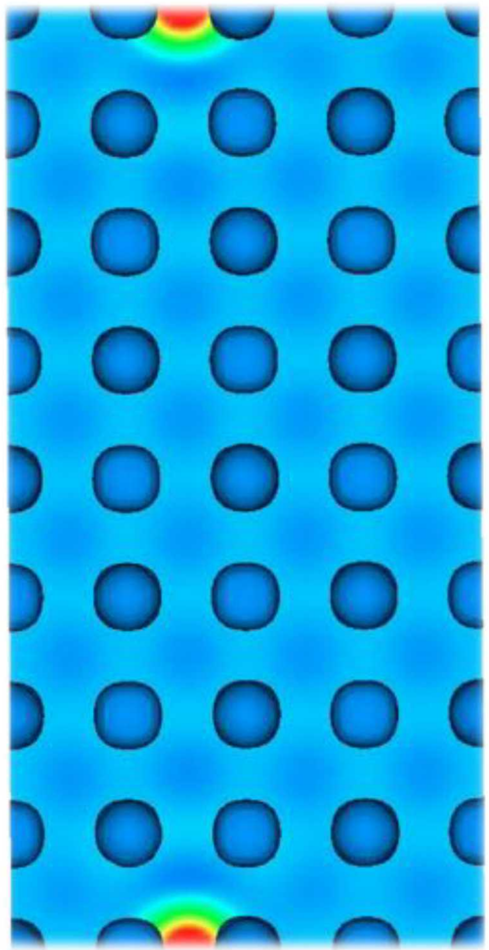

No stopping power
(unphysical)

Ehrenfest MD

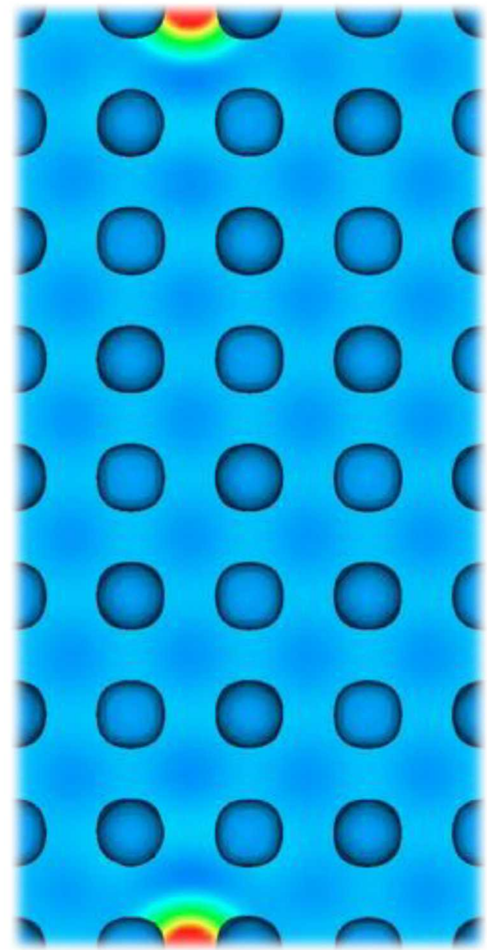

Matches experimental
stopping power

Stopping force

Stopping Power

Warm Dense Deuterium

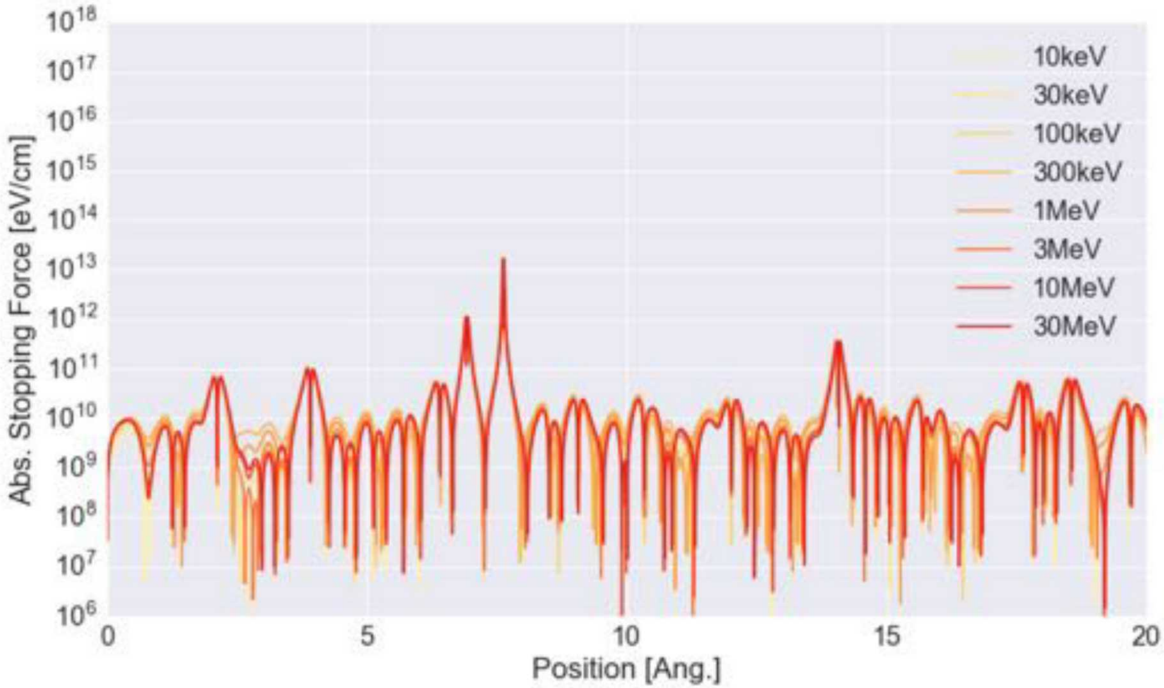

Projectile at 300 keV

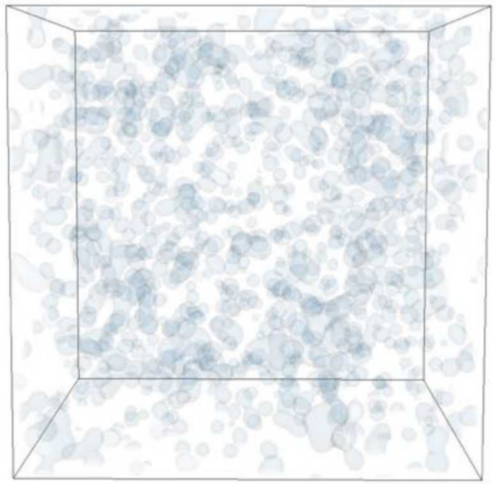

Projectile at 30 MeV

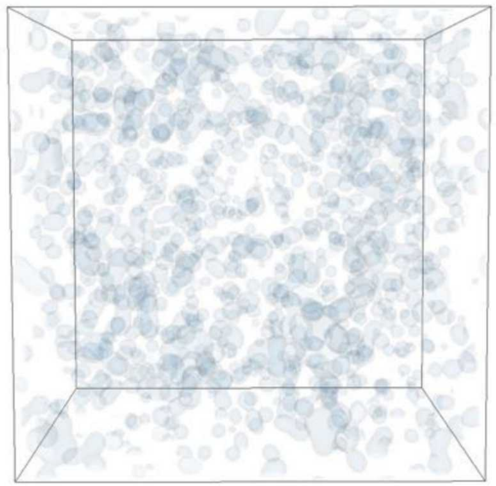

- Stopping at 10 g/cc (mass density) and 2 eV (temperature)
- **Force vs. projectile distance:** Similar across velocities

Stopping Power

Warm Dense Deuterium

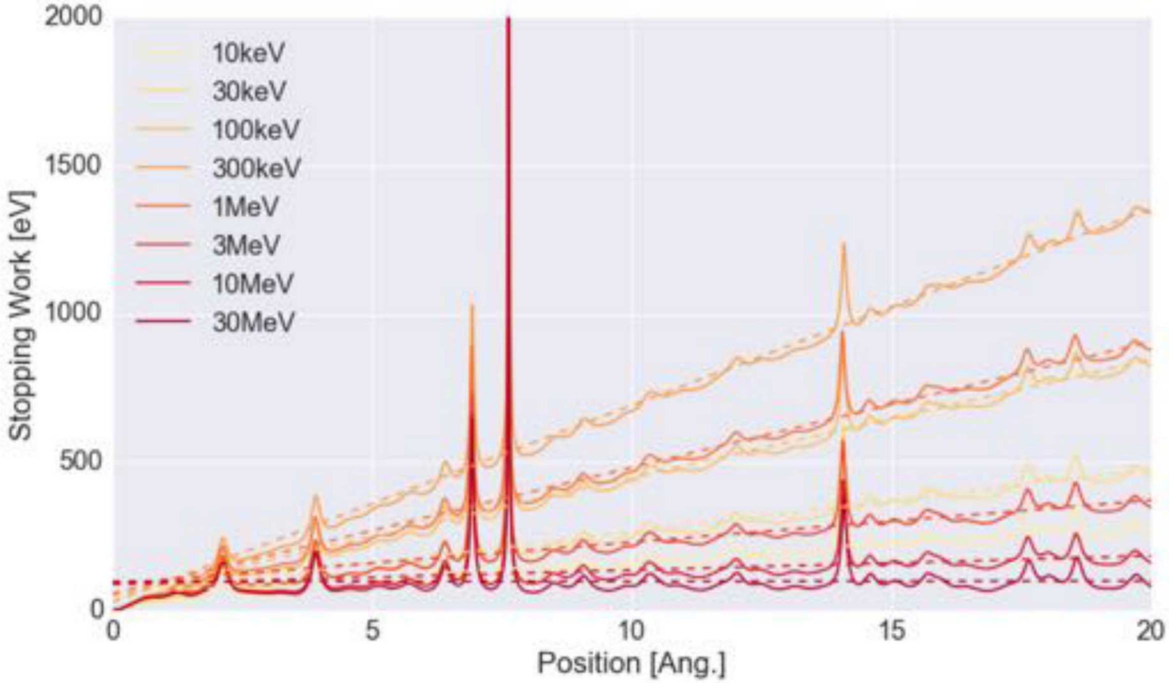

Projectile at 300 keV

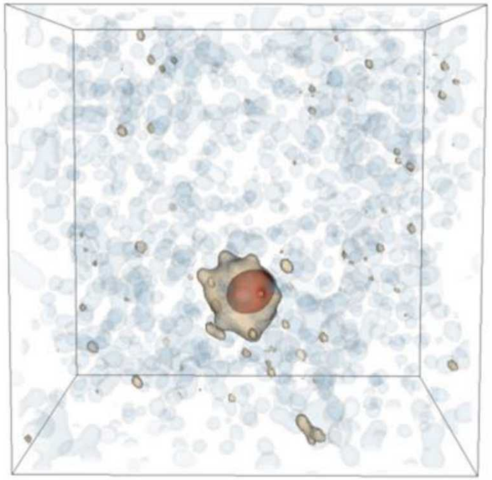

Projectile at 30 MeV

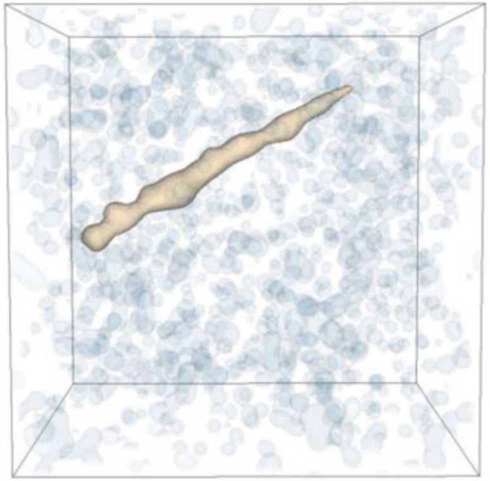

- Stopping at 10 g/cc (mass density) and 2 eV (temperature)
- **Force vs. projectile distance:** Similar across velocities
- **Work vs. projectile distance:** Spikes represent ions

Stopping Power

Warm Dense Deuterium

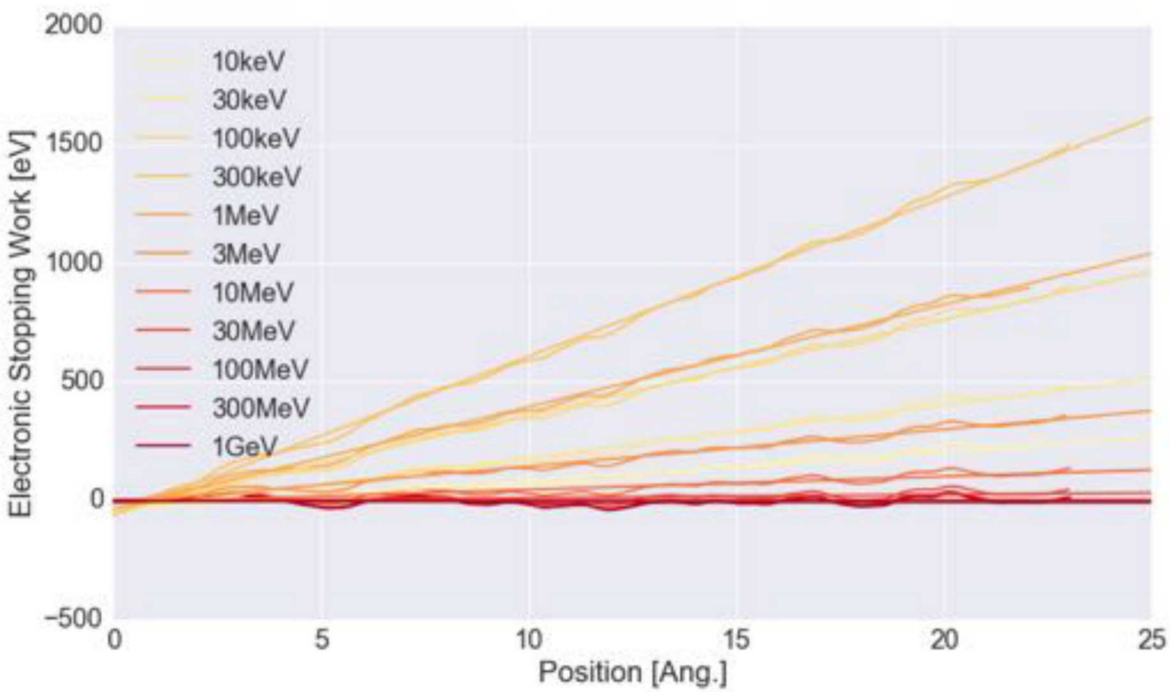

Projectile at 300 keV

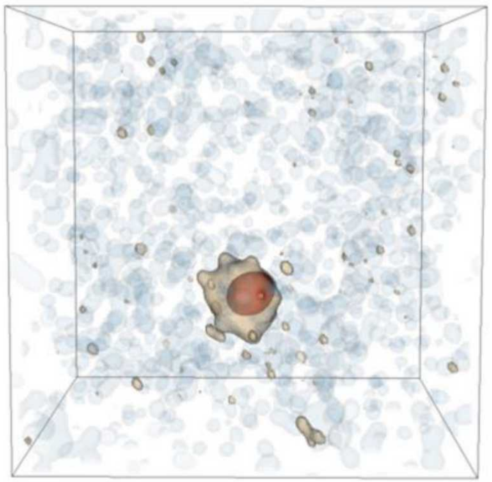

Projectile at 30 MeV

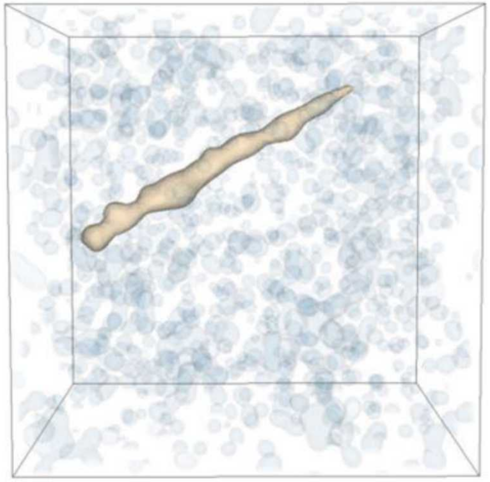

- Stopping at 10 g/cc (mass density) and 2 eV (temperature)
- **Force vs. projectile distance:** Similar across velocities
- **Work vs. projectile distance:** Spikes represent ions
- **Electronic work vs. projectile distance:** Slope represents stopping power

Stopping Power

Warm Dense Deuterium

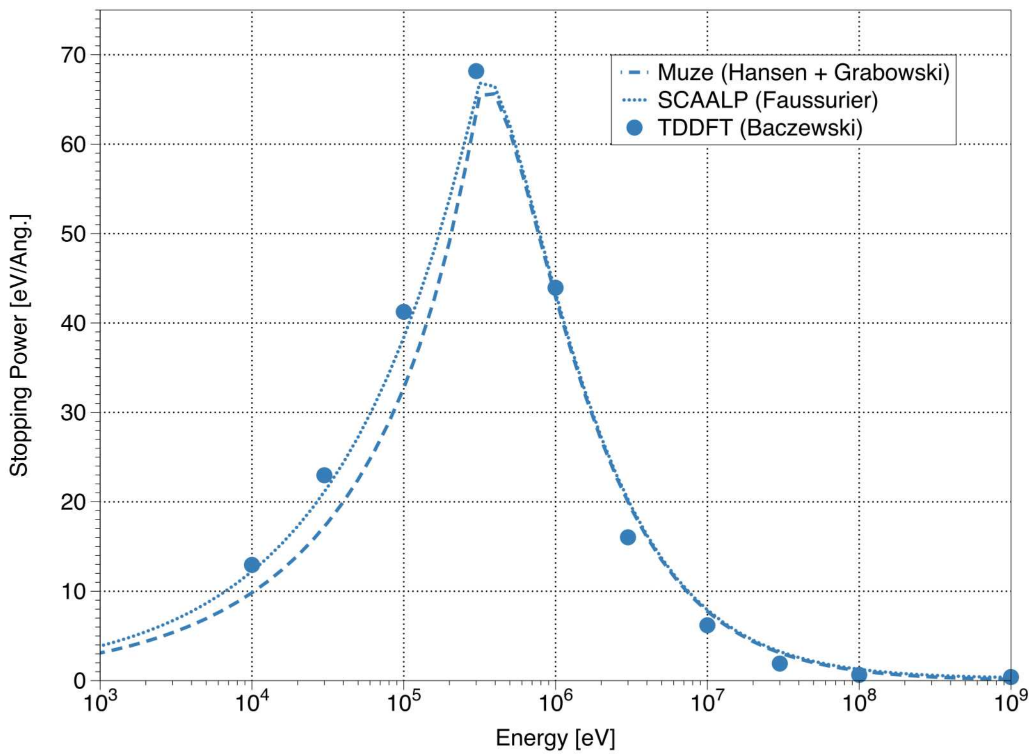

Projectile at 300 keV

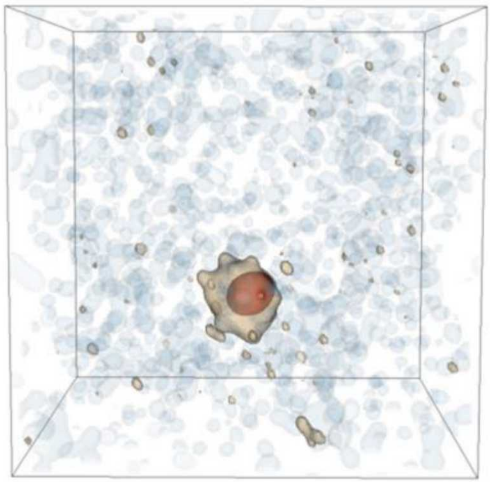

Projectile at 30 MeV

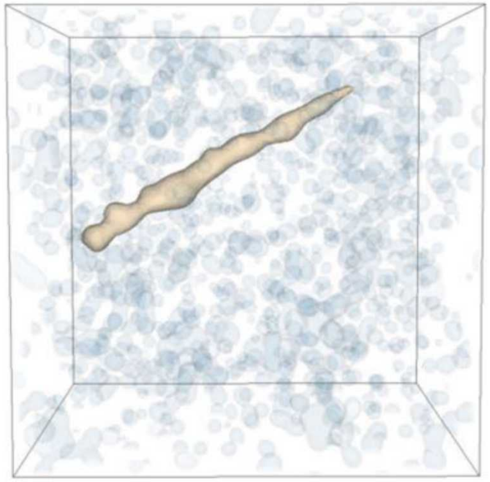

- Stopping at 10 g/cc (mass density) and 2 eV (temperature)
- **Force vs. projectile distance:** Similar across velocities
- **Work vs. projectile distance:** Spikes represent ions
- **Electronic work vs. projectile distance:** Slope represents stopping power

X-Ray Thomson Scattering

The Chihara Decomposition

J. Phys. F: Met. Phys. 17 (1987) 295–304.

Difference in x-ray scattering between metallic and non-metallic liquids due to conduction electrons

Junzo Chihara

Department of Physics, Japan Atomic Energy Research Institute, Tokai, Ibaraki 319-11, Japan

Starting point for most models of the dynamic structure factor

- Partition electrons into bound and free and model each contribution

$$S(\mathbf{q},\omega) = |f_I(\mathbf{q}) + n(\mathbf{q})|^2\, S_{ii}(\mathbf{q},\omega) + Z_f\, S_{ee}(\mathbf{q},\omega) + S_{bf}(\mathbf{q},\omega)$$

In principle, this is fine.

In practice, there can be problems:

- Distinction between bound and free electrons might break down for WDM
- Inconsistent treatment of various terms
- More parameters

X-Ray Thomson Scattering

Chihara-free Dynamic Structure Factor under HED Conditions

Probe system with x-ray

$$v(\mathbf{r},t) = v_0\, e^{i\mathbf{q}\cdot\mathbf{r}} f(t)$$

$$|\mathbf{q}| = \frac{4\pi \sin(\theta/2)}{\lambda_0}$$

λ_0 : probe wavelength (2Å)

Record density response

$$\delta n(\mathbf{q},t) = \int_0^\infty d\tau\ \chi(\mathbf{q},-\mathbf{q},\tau)\, v_0\, f(t-\tau)$$

Apply dissipation-fluctuation theorem

$$\chi(\mathbf{q},-\mathbf{q},\omega) = \frac{\delta n(\mathbf{q},\omega)}{v_0\, f(\omega)}$$

$$S(\mathbf{q},\omega) = -\frac{1}{\pi}\frac{\Im\left[\chi(\mathbf{q},-\mathbf{q},\omega)\right]}{1-e^{-\omega/k_{\mathrm{B}}T}}$$

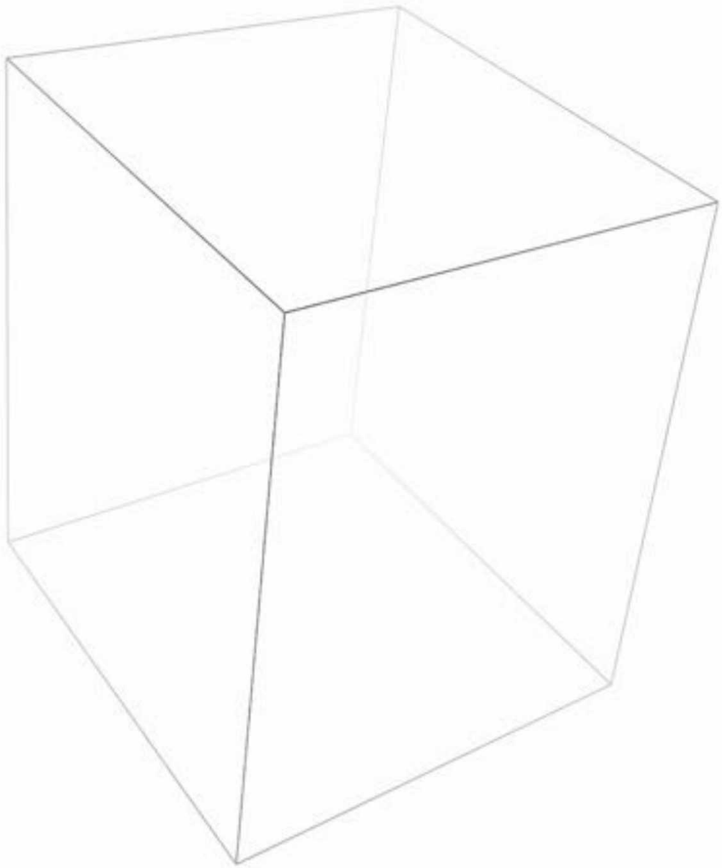

X-Ray Thomson Scattering

Chihara-free Dynamic Structure Factor under HED Conditions

Probe system with x-ray

$$v(\mathbf{r},t) = v_0\, e^{i\mathbf{q}\cdot\mathbf{r}} f(t)$$

$$|\mathbf{q}| = \frac{4\pi \sin(\theta/2)}{\lambda_0}$$

λ_0 : probe wavelength (2Å)

Record density response

$$\delta n(\mathbf{q},t) = \int_0^\infty d\tau\ \chi(\mathbf{q},-\mathbf{q},\tau)\, v_0\, f(t-\tau)$$

Apply dissipation-fluctuation theorem

$$\chi(\mathbf{q},-\mathbf{q},\omega) = \frac{\delta n(\mathbf{q},\omega)}{v_0\, f(\omega)}$$

$$S(\mathbf{q},\omega) = -\frac{1}{\pi}\frac{\Im\left[\chi(\mathbf{q},-\mathbf{q},\omega)\right]}{1-e^{-\omega/k_\mathrm{B}T}}$$

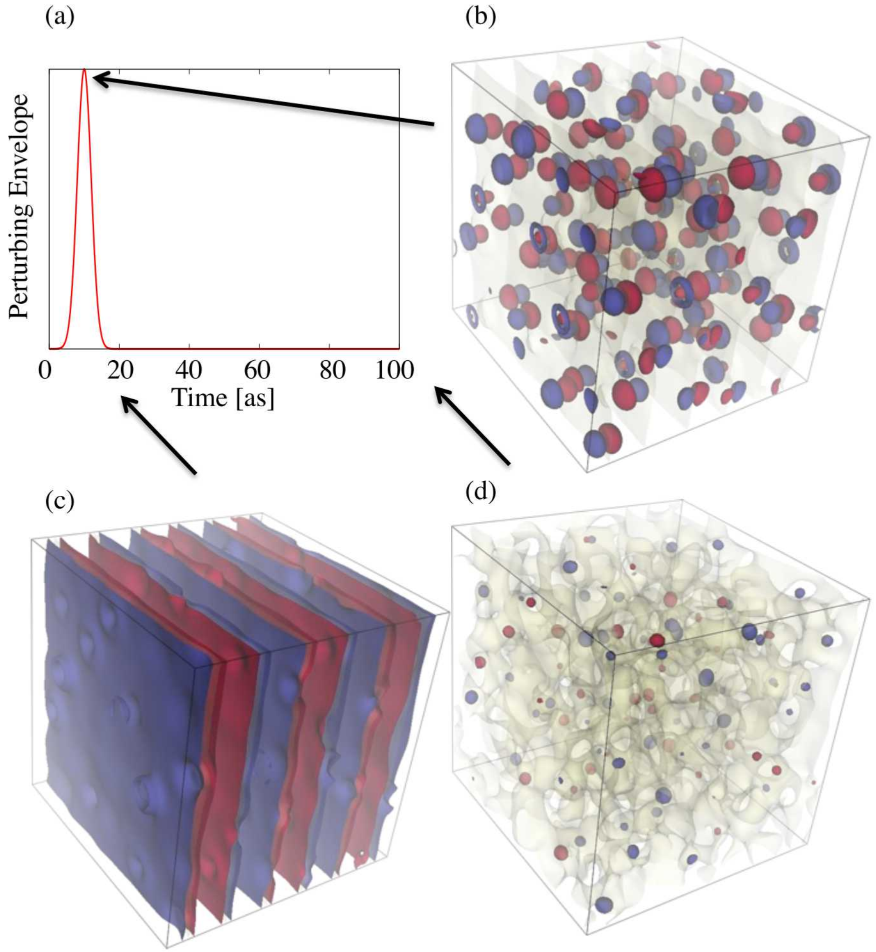

X-Ray Thomson Scattering

Chihara-free Dynamic Structure Factor under HED Conditions

Comparison of TDDFT (solid lines) to state-of-the-art models

- **Free electron feature**
  RPA dielectric function and Mermin approximation (dashed)

$$\frac{d^2\sigma}{d\Omega d\omega} = \sigma_T \frac{q_s}{q_i} S(q,\omega)$$

$$S(q,\omega) = -\frac{k^2}{4\pi^2 n_e} \frac{\mathrm{Im}\left[\epsilon^{-1}(q,\omega)\right]}{1-\exp(-\omega/T_e)}$$

$$\epsilon^M(q,\omega) - 1 = \frac{\left(1 + i\frac{\nu(\omega)}{\omega}\right)\left[\epsilon^{RPA}(q,\omega+i\nu(\omega)) - 1\right]}{1 + i\frac{\nu(\omega)}{\omega}\frac{\epsilon^{RPA}(q,\omega+i\nu(\omega))-1}{\epsilon^{RPA}(q,0)-1}}$$

- **Bound-free feature**
  Average-atom ion-sphere model with Slater exchange (dashed lines)

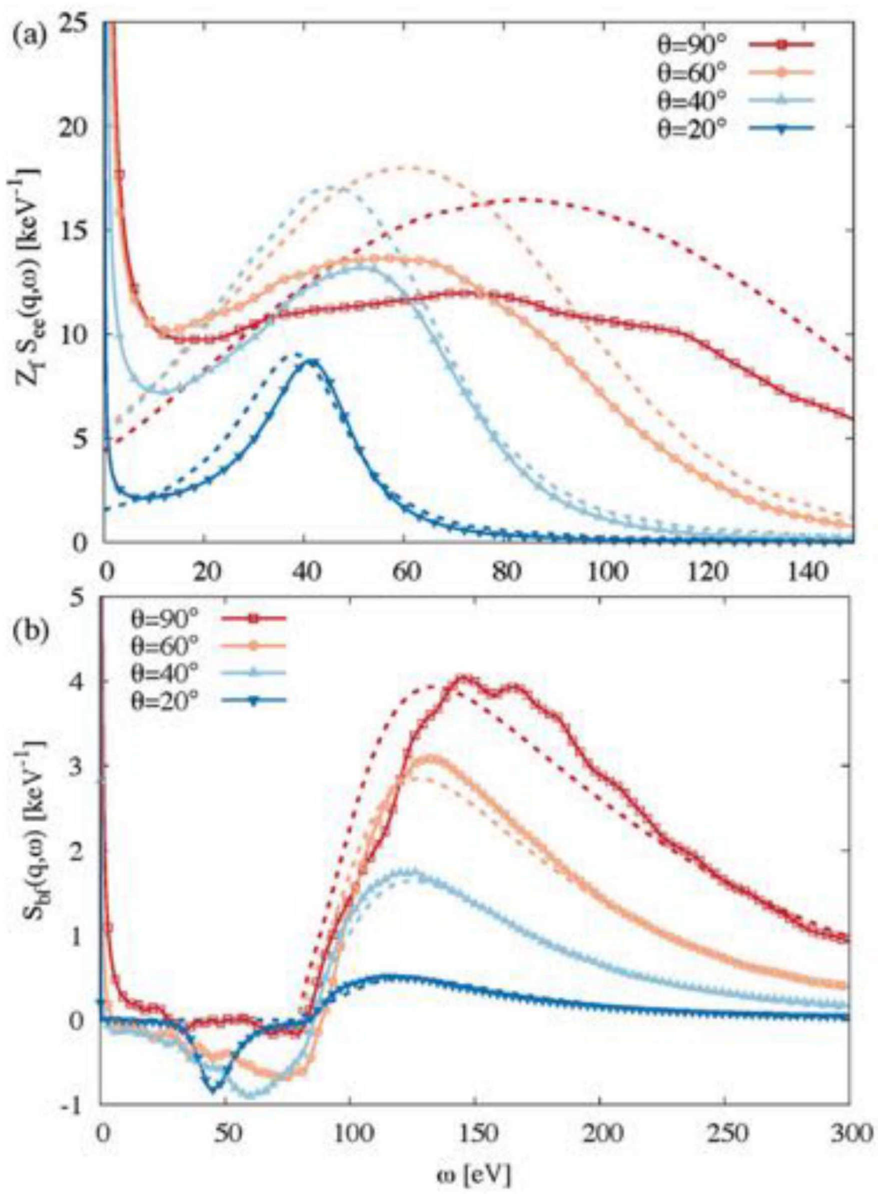

Electrical and Optical Conductivity under HED Conditions

Liquid Aluminum at High Temperature

State-of-the art conductivities from static approaches (average-atom methods or DFT with Kubo-Greenwood formula)

$$\sigma_{\mathbf{k}}(\omega) = \frac{2\pi}{3\omega\Omega} \sum_{i,j} [f(\epsilon_{i,\mathbf{k}}) - f(\epsilon_{j,\mathbf{k}})]$$
$$\times |\langle \phi_{j,\mathbf{k}} | \nabla | \phi_{j,\mathbf{k}} \rangle|^2 \delta(\epsilon_{j,\mathbf{k}} - \epsilon_{i,\mathbf{k}} - \omega)$$

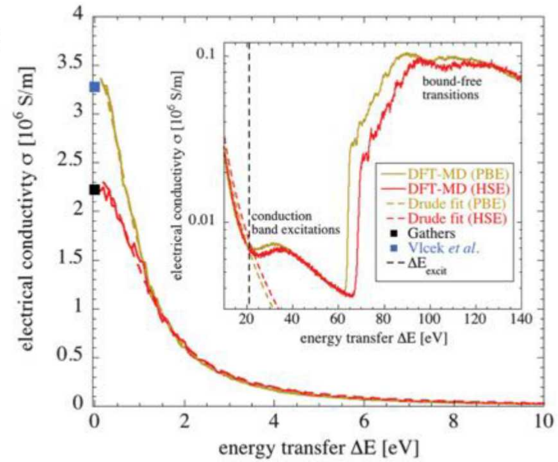

B. B. L. Witte et al., Phys. Rev. Lett. **118**, 225001 (2017).

Going beyond static approaches with TDDFT

- No abuse of KS quantities
- Better scaling than in the energy domain
- Beyond linear response

$$\mathbf{E}(t) = -\frac{1}{c}\frac{\partial \mathbf{A}(t)}{\partial t}$$
$$\mathbf{J}(t) = -\frac{i}{\Omega}\int d^3r \sum_j \phi_j^*(\mathbf{r},t) \left[\hat{H}(t), \hat{\mathbf{r}}\right] \phi_j(\mathbf{r},t)$$
$$\mathbf{J}(\omega) = \sigma(\omega)\, \mathbf{E}(\omega)$$

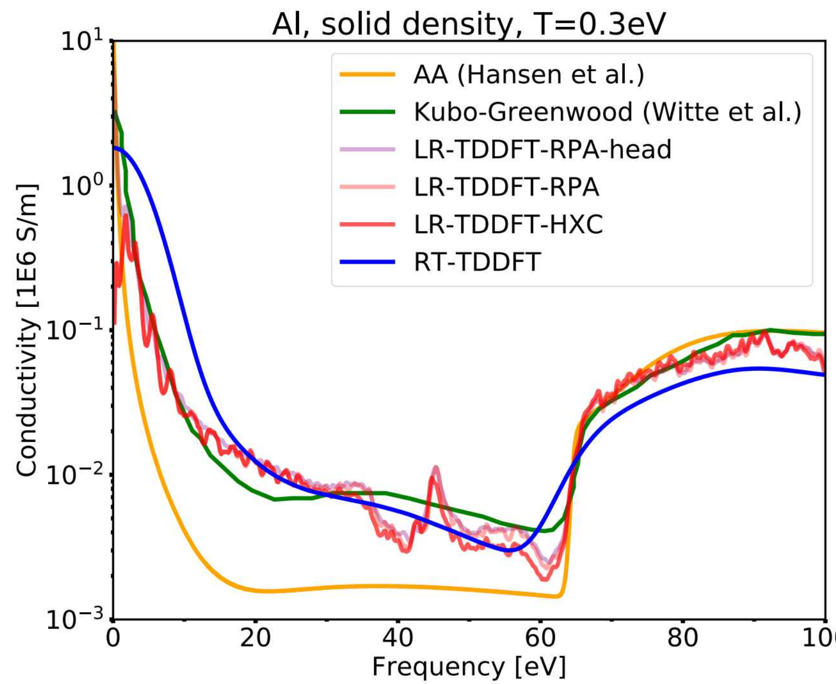

A. Cangi et al., in prep. (2018).

Conclusions and Outlook

First-principle TDDFT calculations provide microscopic data and help constrain experiments and other state-of-the-art models.

Stopping power

- Capability to improve databases of stopping curves for a wide range of warm dense targets (mixtures of target materials, different types of projectiles, statistical data)

X-ray Thompson scattering / Conductivities

- Capability to help with diagnostics and serve as input to magneto-hydrodynamics simulations.

Future developments

- Need for a self-consistent model for HED physics
- Need for improvements in computational efficiency and accuracy
- Computationally efficient stopping power with TDDFT on average-atom models
- Thermal conductivity from TDDFT
- More accurate inclusion of non-adiabatic effects from the exact factorization method
- Non-equilibrium many-body perturbation theory

Backup slides

Introduction

What are HED and WDM conditions?

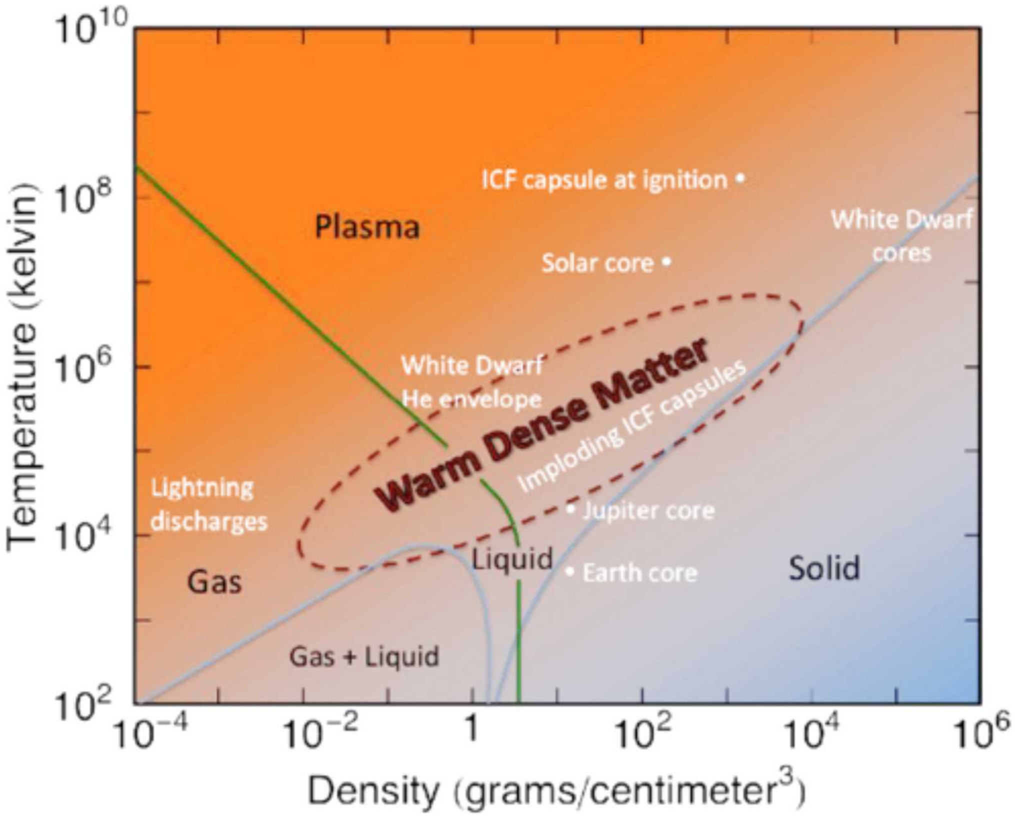

Basic Research Needs for HEDLP, Report of the Workshop on HEDLP Research Needs, DOE (2008).

Coulomb coupling parameter

$$\Gamma = \frac{V}{T} = \frac{Ze^2}{r_\mathrm{S} k_\mathrm{B} \tau}$$

Electron degeneracy parameter

$$\Theta = \frac{k_\mathrm{B}\tau}{E_\mathrm{F}}$$

Warm dense matter regime

$$\Gamma \approx 1\,, \quad \Theta \approx 1$$

Introduction

High energy density (HED) conditions

Creating HED conditions requires transferring an enormous amount of energy to a target in a very short period of time.

Compression of energy in time and space in pulsed power facilities (Z machine) enables exciting science (astrophysics, planetary science, inertial confinement fusion).

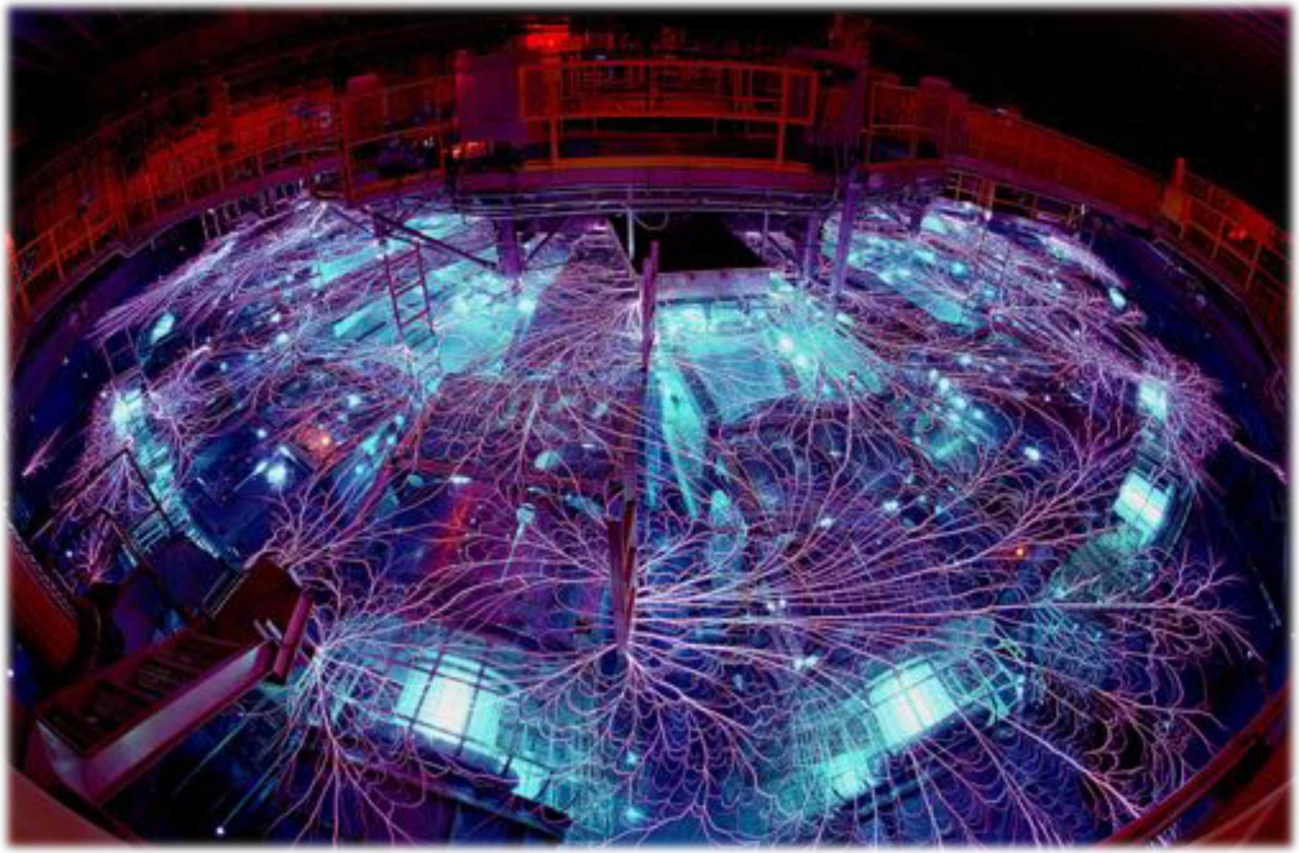

Z Machine, Sandia National Laboratories.

Introduction

Time scales

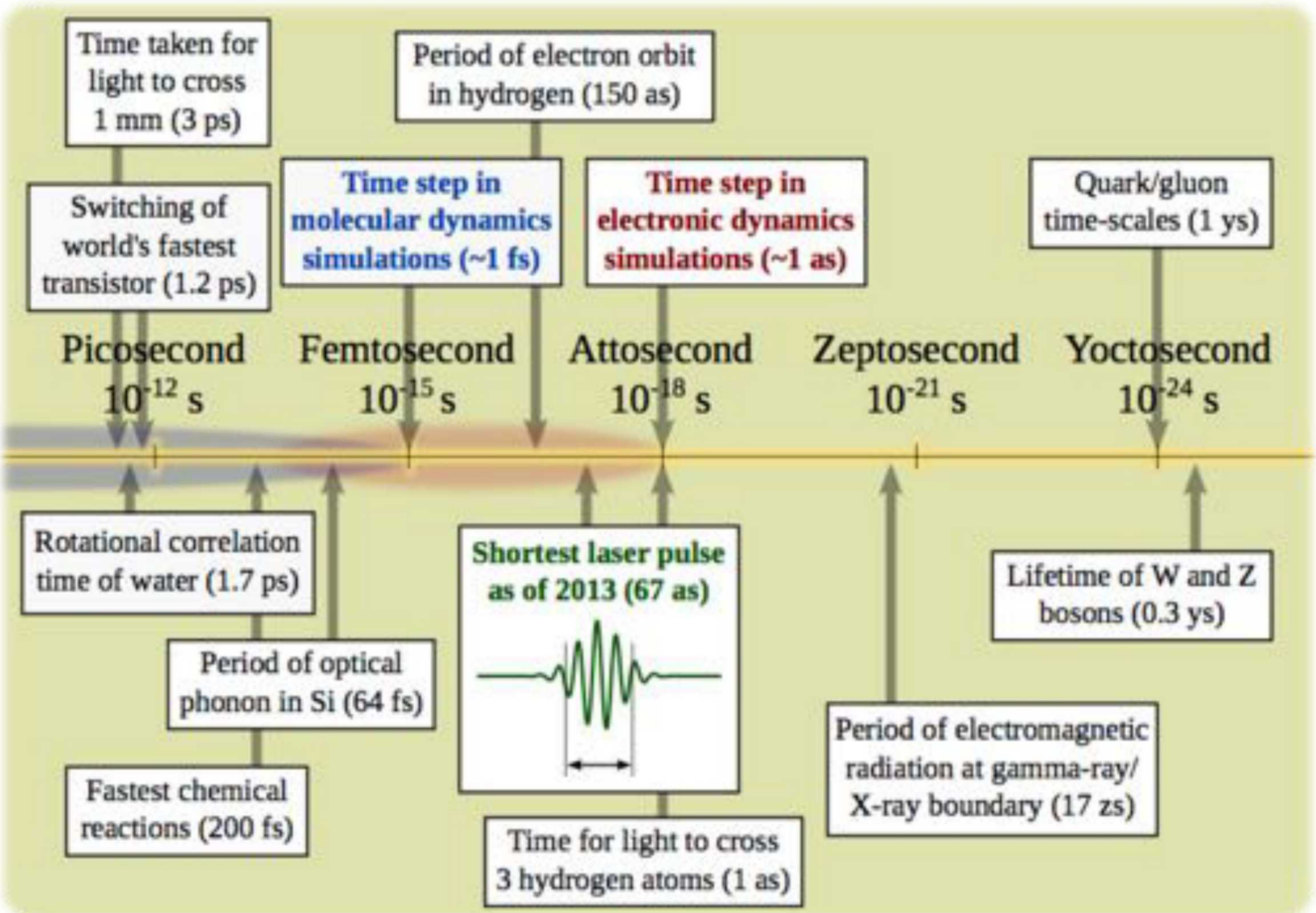

Courtesy of Kay Dewhurst, Max Planck Institute of Microstructure Physics (2015).

Theoretical Background

Density Functional Theory

Electronic Hamiltonian	$\hat{H} = \hat{T} + \hat{V}_{\mathrm{ee}} + \hat{V}$
Hohenberg-Kohn functional	$F[n] = \min_{\hat{\Psi} \to n} \langle \Psi \vert \hat{T} + \hat{V}_{\mathrm{ee}} \vert \Psi \rangle$ $E_v = \min_n \left\{ F[n] + \int d\mathbf{r}\; n(\mathbf{r})\, v(\mathbf{r}) \right\}$
Kohn-Sham scheme	$\left\{ -\frac{\nabla^2}{2} + v_{\mathrm{S}}(\mathbf{r}) \right\} \phi_i(\mathbf{r}) = \epsilon_i \phi_i(\mathbf{r})$ $n(\mathbf{r}) = \sum_i^N \phi_i^*(\mathbf{r}) \phi_i(\mathbf{r})$ $F[n] = T_{\mathrm{S}}[n] + U[n] + E_{\mathrm{XC}}[n]$ $v_{\mathrm{S}}(\mathbf{r}) = v(\mathbf{r}) + \frac{\delta U[n]}{\delta n(\mathbf{r})} + \frac{\delta E_{\mathrm{XC}}[n]}{\delta n(\mathbf{r})}$

Theoretical Background
Density Functional Theory (at finite temperature)

Electronic Hamiltonian	$\hat{H} = \hat{T} + \hat{V}_{\mathrm{ee}} + \hat{V}$ $\hat{\Gamma} = \sum_{N,i} w_{N,i} \lvert\Psi_{N,i}\rangle \langle\Psi_{N,i}\rvert$
Grand potential	$\hat{\Omega} = \hat{H} + \tau\hat{S} + \mu\hat{N}$
Mermin generalization	$F^\tau[n] = \min_{\hat{\Gamma}\to n} \left\{T[\hat{\Gamma}] + V_{\mathrm{ee}}[\hat{\Gamma}] - \tau S[\hat{\Gamma}]\right\}$ $\Omega^\tau_{v-\mu} = \min_n \left\{F^\tau[n] + \int d\mathbf{r}\; n(\mathbf{r})\; (v(\mathbf{r}) - \mu)\right\}$
Kohn-Sham scheme	$\left\{-\frac{\nabla^2}{2} + v^\tau_{\mathrm{S}}(\mathbf{r})\right\} \phi_i(\mathbf{r}) = \epsilon^\tau_i \phi_i(\mathbf{r})$ $n(\mathbf{r}) = \sum_i^N f^\tau_i \phi^*_i(\mathbf{r})\phi_i(\mathbf{r})\,, \quad f^\tau_i : \mathrm{FD}$ $F^\tau[n] = T^\tau_{\mathrm{S}}[n] - \tau S^\tau[n] + U^\tau[n] + E^\tau_{\mathrm{XC}}[n]$ $v^\tau_{\mathrm{S}}(\mathbf{r}) = v(\mathbf{r}) + \frac{\delta U^\tau[n]}{\delta n(\mathbf{r})} + \frac{\delta E^\tau_{\mathrm{XC}}[n]}{\delta n(\mathbf{r})}$

Application 1: Stopping Power
Electronic Stopping in Warm Dense Targets

Stopping mechanisms
- Nuclear stopping (lattice vibrations)
- Electronic stopping (electronic excitations)

Large body of literature for cold targets
- Empirical approximations (*Rutherford, Thomson, Bohr, Bethe*)
- Parameter-free atomistic simulations
  - Electronic structure coupled to molecular dynamics
  - Cold stopping power (*Echenique, Correa, Artacho, Schleife*)

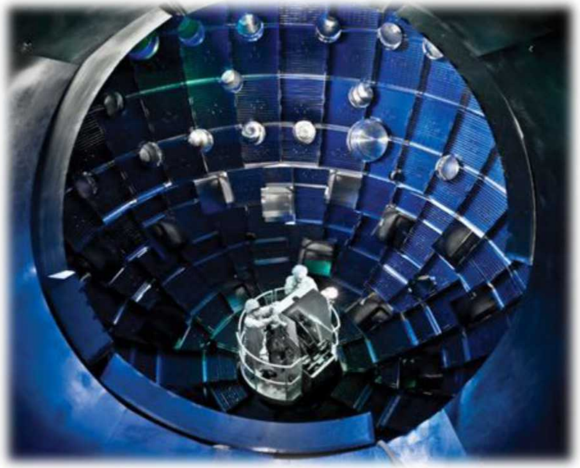

Target chamber, National Ignition Facility, Lawrence Livermore National Laboratories.

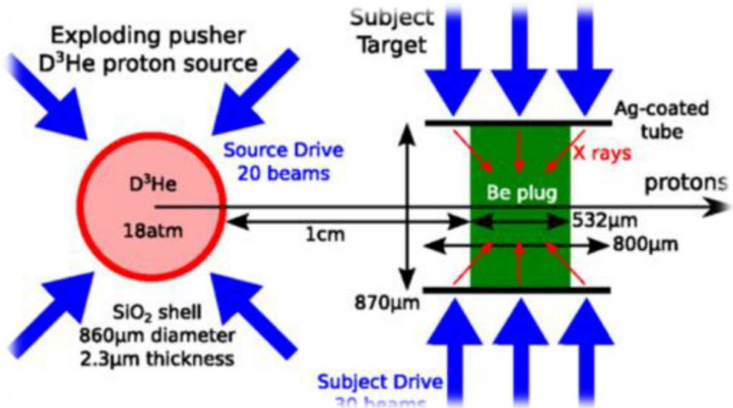

Zylstra et al., Phys. Rev. Lett. **114**, 215002 (2015).

Application 1: Stopping Power

H/Be Stopping Simulation

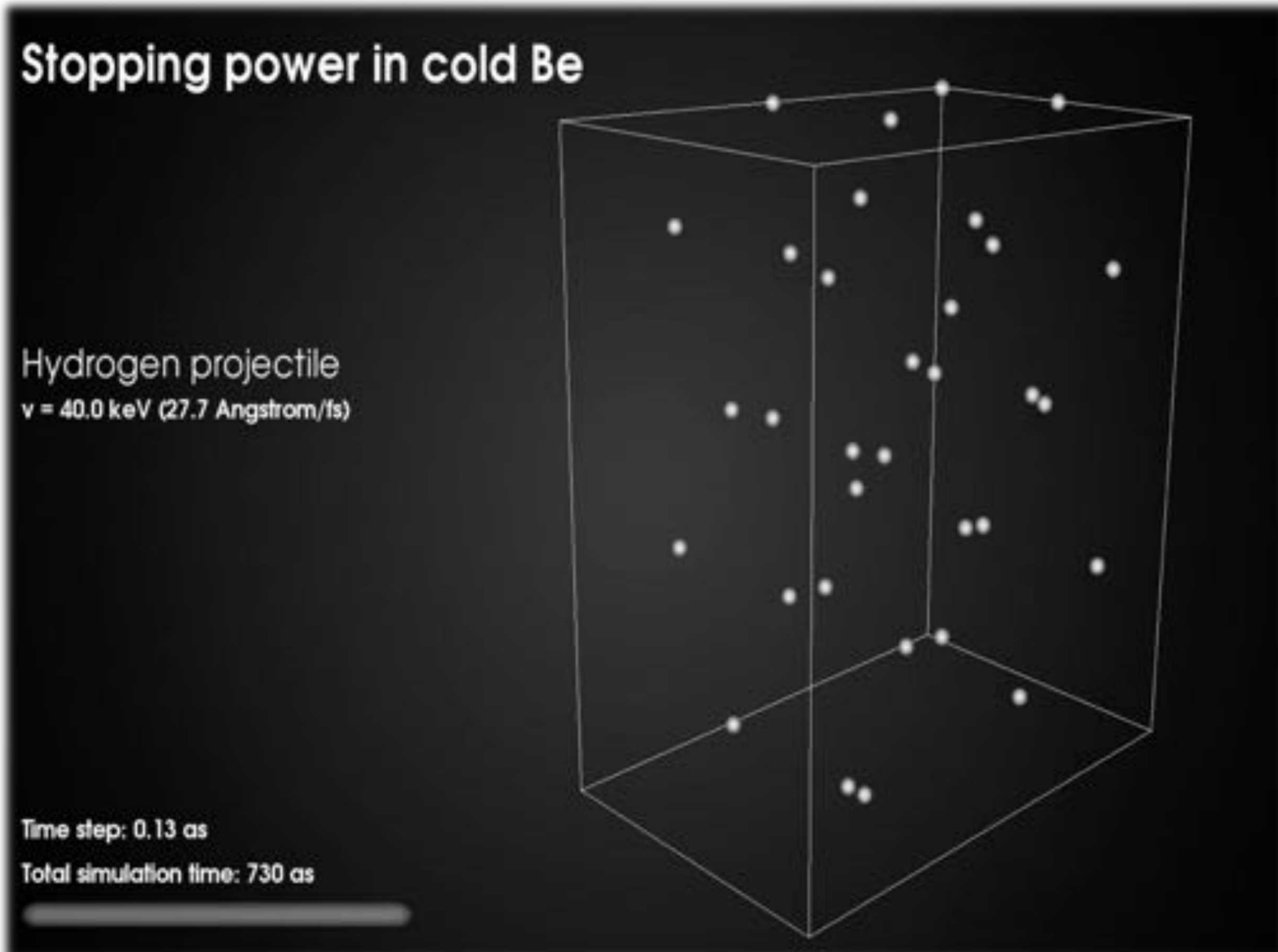

Application 1: Stopping Power

H/Be Stopping Simulation: Electronic Stopping Force

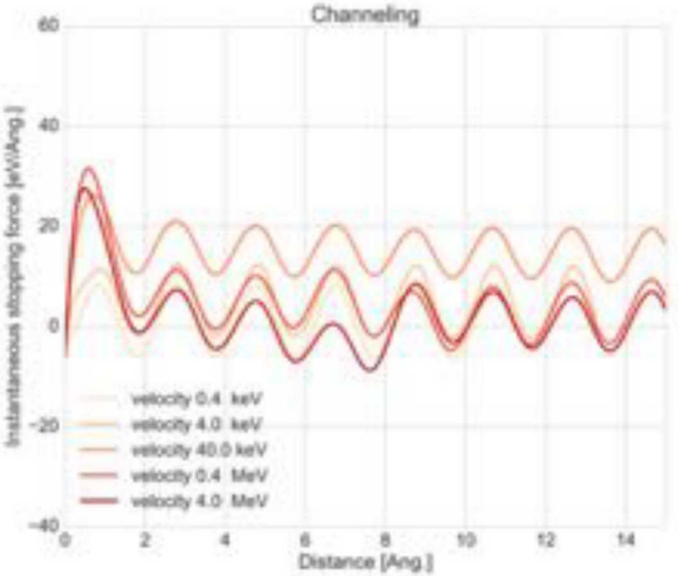

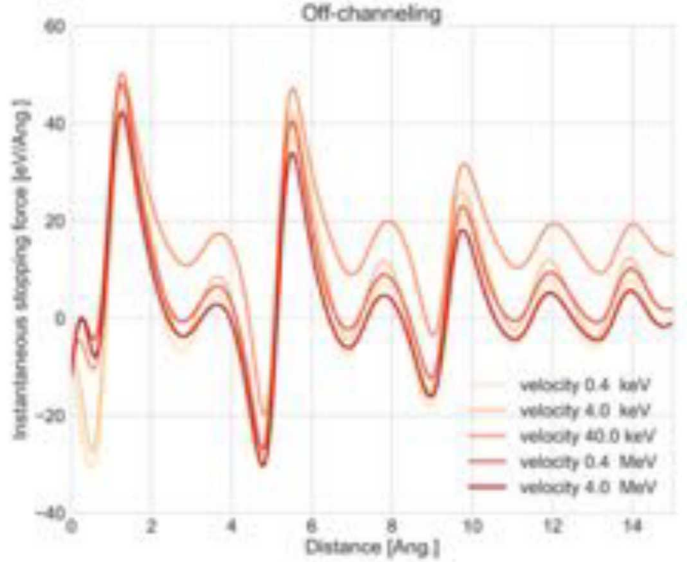

Application 1: Stopping Power

Microscopic Statistics of the Electronic Stopping Force

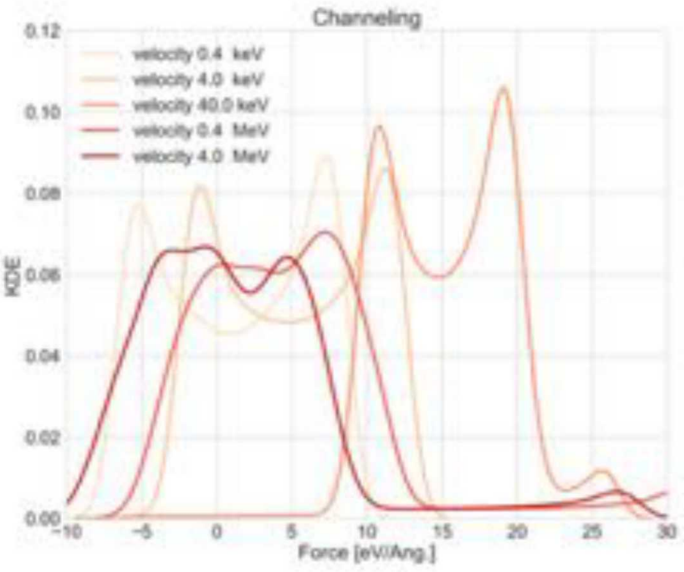

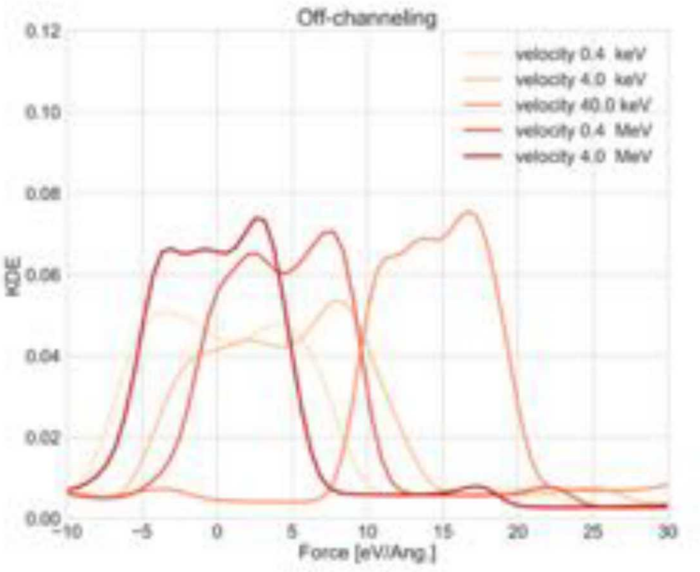

Application 1: Stopping Power

H/Be Stopping Simulation: Electronic Stopping Work

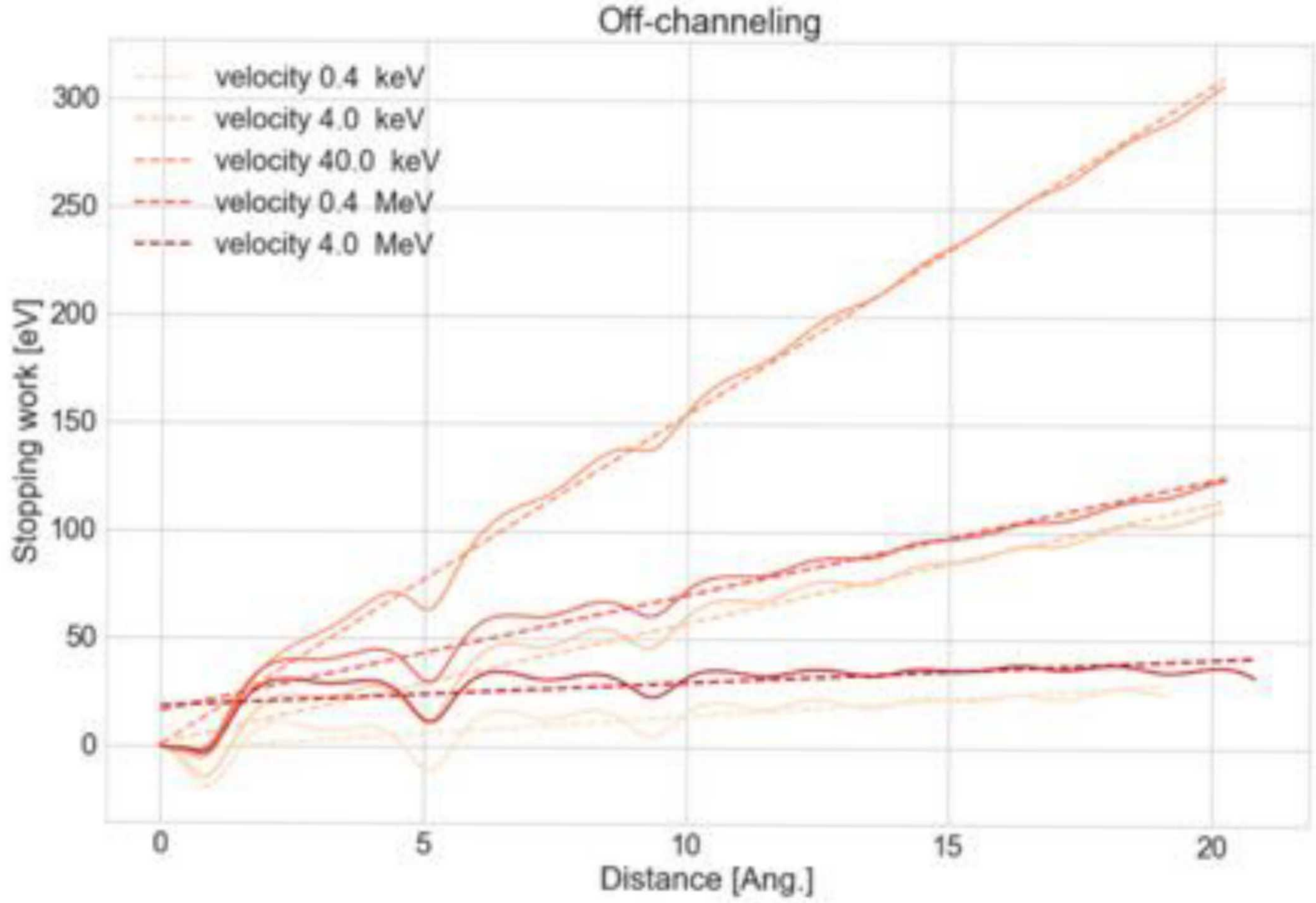

Application 1: Stopping Power

Cold and Warm Dense Beryllium

Calculations performed on ***Solo***
(5 nodes, 32 cores per node, 1 day)

Calculations performed on ***Sequoia***
(3000 nodes,16 cores per node, 1 day)

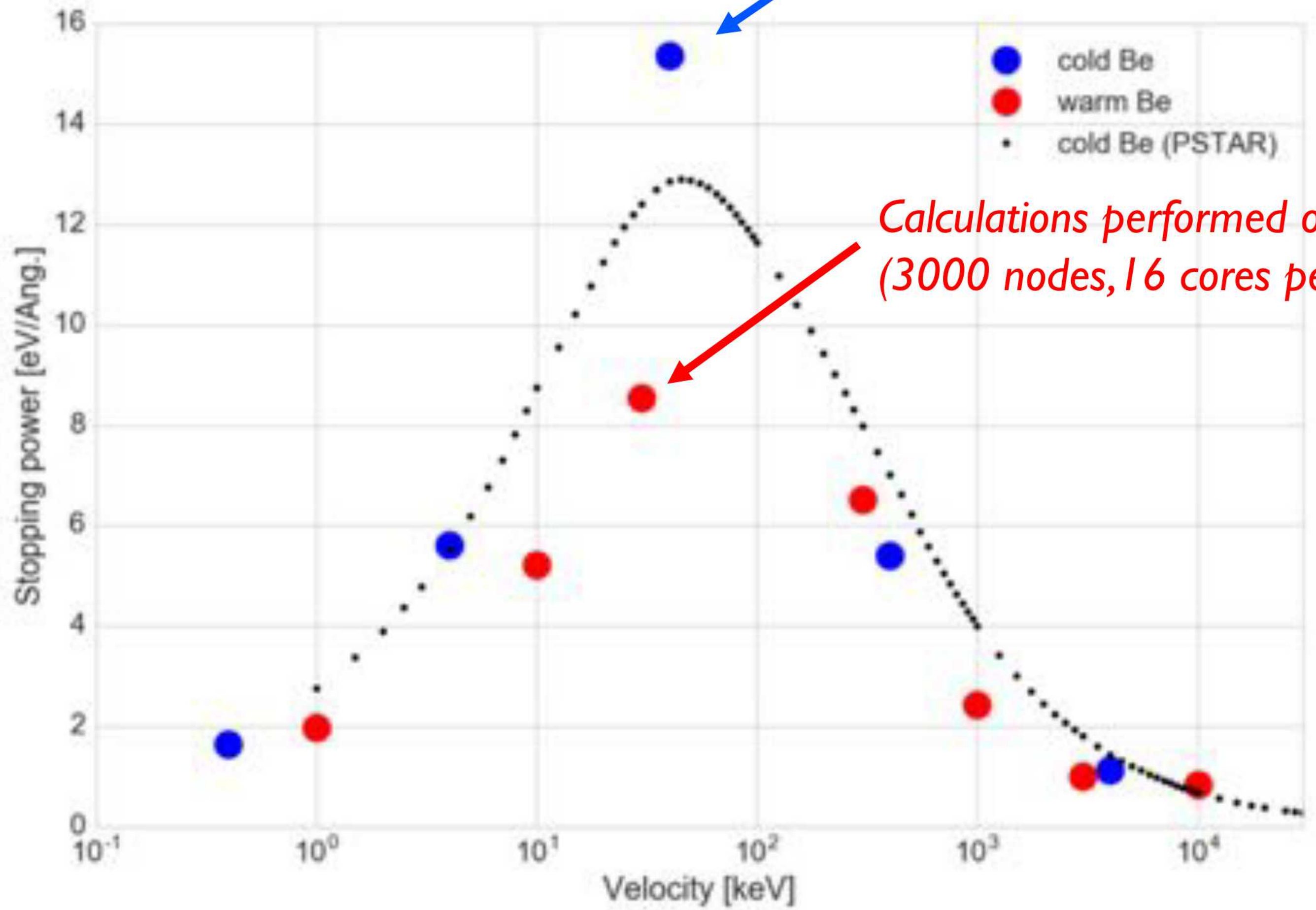

Application 1: Stopping Power

Stopping in Warm Dense Deuterium: A Closer Look

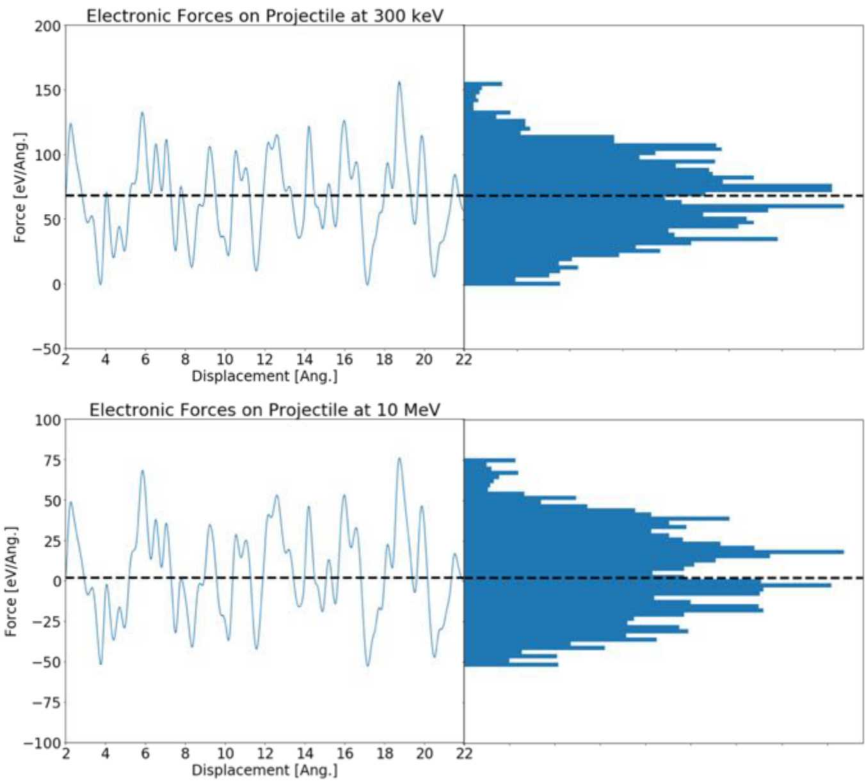

Projectile at 300 keV

Projectile at 30 MeV

- Stopping at 10 g/cc (mass density) and 2 eV (temperature)
- **Force vs. projectile distance:** Similar across velocities
- **Microscopic distribution** of forces: More data

Application 2: X-Ray Thompson Scattering

A Concise Introduction

Hard x-rays

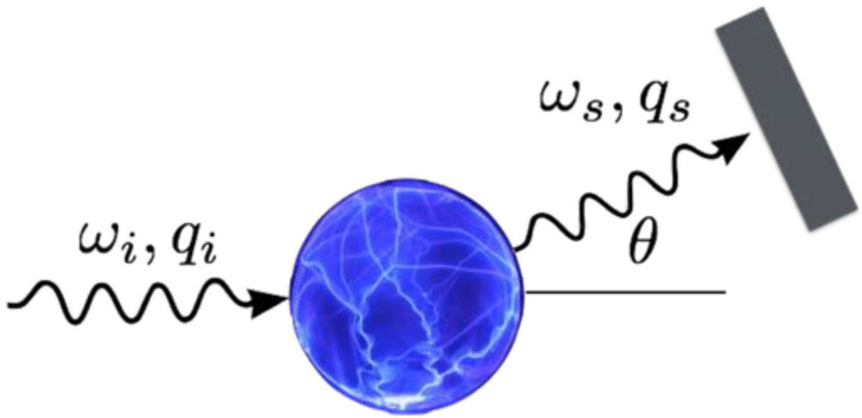

Measure inelastically scattered x-rays

Sample of WDM
(opaque to optical probes)

$$\omega = \omega_i - \omega_s$$

$$q = q_i - q_s$$

$$q_s = 2q_i \sin(\theta/2)$$

- X-ray Thompson scattering probes density, ionization state, structure, temperature, etc.

X-ray Thomson scattering in high energy density plasmas

Siegfried H. Glenzer and Ronald Redmer
Rev. Mod. Phys. **81**, 1625 – Published 1 December 2009

- Cross section is proportional to dynamic structure factor $\frac{d^2\sigma}{d\Omega d\omega} = \sigma_T \frac{q_s}{q_i} S(q, \omega)$

Application 2: X-Ray Thompson Scattering

Supporting diagnostics of LCLS with TDDFT

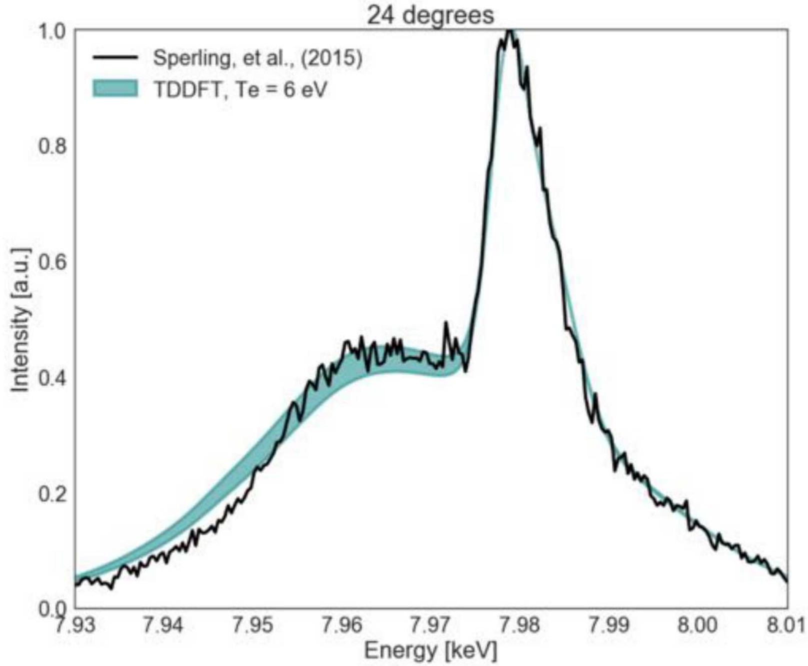

Free-Electron X-Ray Laser Measurements of Collisional-Damped Plasmons in Isochorically Heated Warm Dense Matter

P. Sperling, E. J. Gamboa, H. J. Lee, H. K. Chung, E. Galtier, Y. Omarbakiyeva, H. Reinholz, G. Röpke, U. Zastrau, J. Hastings, L. B. Fletcher, and S. H. Glenzer
Phys. Rev. Lett. **115**, 115001 – Published 9 September 2015

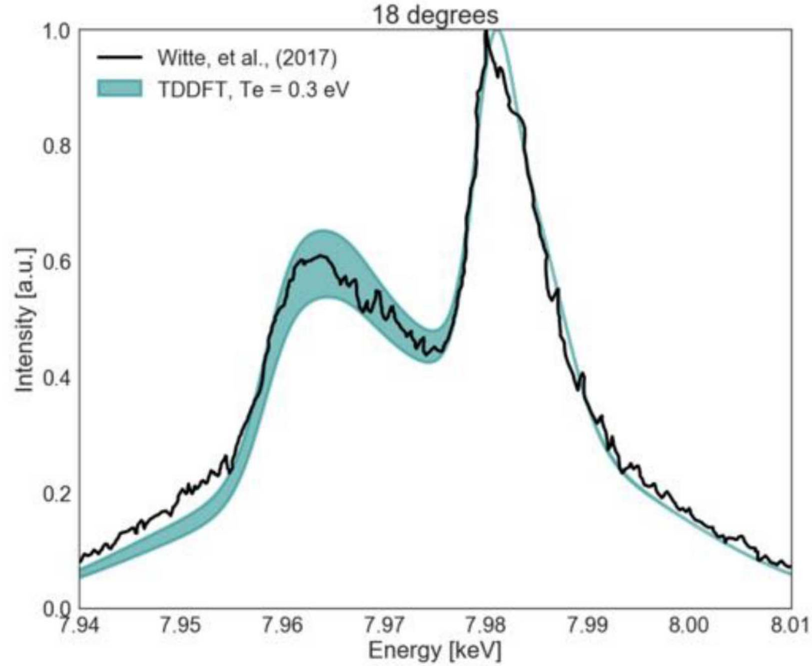

Warm Dense Matter Demonstrating Non-Drude Conductivity from Observations of Nonlinear Plasmon Damping

B. B. L. Witte, L. B. Fletcher, E. Galtier, E. Gamboa, H. J. Lee, U. Zastrau, R. Redmer, S. H. Glenzer, and P. Sperling
Phys. Rev. Lett. **118**, 225001 – Published 31 May 2017